Representations of Three-Body Interactions In Physics

by Joel Johansen

Thesis submitted for the degree of
Bachelor of Physics
Project duration: II months

Supervisor: Gillis Carlsson
Co-supervisor: Andrea Idini

LUND
UNIVERSITY

Department of Physics
Division of Mathematical Physics
Date: May 2023

Abstract. The thesis explores an already developed symmetry adapted representation of a two-body interaction with the main goal of extending the method to also include three-body interactions. The method considers a space of shifted one dimensional Gaussian particle densities which are used, together with their corresponding Hartree potentials, to define the respective collective subspaces in which the interactions are expanded. The performance of the method is then examined by how much the interactions can be compressed at the expense of the resolution in the potential energy of particle densities modeled by one dimensional Gaussian distributions. By compression, the percentage reduction in numerical calculations is meant. The result shows that the method is successful in compressing two and three-body interactions by about 94 and 97 % respectively, while still allowing the interactions to be fully recovered in their collective subspaces.

Contents

Notation and List of Abbreviations

Below is list of abbreviations used throughout the text.

- SVD – Singular Value Decomposition.
- HOSVD – Higher-Order Singular Value Decomposition.
- RMSLE – Root-Mean-Square-Logarithmic Error.
- LAE – Logarithmic-Absolute Error

Tensors are denoted by calligraphic capital letters ($\mathcal{A}$, $\mathcal{B}$, ...), matrices are written in bold capital letters ($\mathbf{A}$, $\mathbf{B}$, ...) while scalars are represented by ordinary lowercase letters (a, b, ...). Entries of tensors/matrices are similarly denoted by ordinary letters, but with an additional subscript indicating the position of the element along the axes of the tensor/matrix. The English (Latin) and Greek alphabet are both used.

1 Introduction

The primary goal of physics is to find the fundamental laws that govern the behavior of our universe. This is indeed possible in areas such as classical mechanics and optics, where a few unifying concepts can be used to explain nearly all observed phenomena. The same can not be said about nuclear physics, however, where the underlying principles determining basic properties of nuclear matter, such as the binding energy or density of nuclei, are still being uncovered. The fundamental theory of strong interactions is notoriously difficult to solve in the low energy regime, as a result, solving the many-body nuclear problem from first principles becomes extremely challenging.

In order to resolve this issue, one usually has to resort to effective field theories, where the appropriate degrees of freedom are restricted and expanded. Typically, in the context of nuclear physics at least, such effective theories features both two and higher-body forces. The two-body force is generally defined to act as the main contributor, with three and higher-body forces giving gradually smaller corrections. Although, there is evidence that three-body forces might have a significant contribution to the binding energy in light nuclei [1].

Calculations involving three-body forces dates back to the mid fifties [2][3] and has led to the formation of several effective theories adopting the three-body formalism. The perhaps most prominent such theory is the Skyrme interaction [4]. The three-body force then takes the form of a repulsive contact interaction, modeled by a zero-range delta potential. However, effective theories featuring a finite-range three-body term has also been suggested [5].

Three-body forces appears in many other areas of physics as well. For instance, in celestial mechanics, three-body tidal forces arise if the bodies are treated as point particles rather than as extended objects, even though gravity only acts pairwise between individual particles. Another example is the Effimov effect, a phenomenon displayed by three-body systems in which resonant two-body forces causes a spectrum of three-body bound states to appear [6] [7].

Practical calculations involving these many-body forces can, however, be computationally hefty, especially calculations concerning three-body forces. It is therefore imperative to have reliable methods that allows one to simulate realistic systems in an efficient way. One such method, which utilizes a symmetry adapted representation of two-body interactions, has recently been developed [8]. The primary goal of this thesis is to extend this method to also treat three-body interactions as well as to further study this earlier work. It will be of particular interest to explore to what degree the resolution of three-body interactions can be optimized to allow for advanced many-body calculations.

We will only consider local two and three-body interactions that are independent of both spin and isospin, which, admittedly, limits the use of the method in its current state. In particular, we will use finite-ranged Gaussian potentials, although, the method is very general and works equally well no matter the spacial dependence. Additionally, we will restrict ourselves to work in one dimension, though, in [8] the problem is fully treated in three dimensions. In order to simplify matters further, kinetic terms will also be disregarded.

The results shows that the two and three-body interactions can each be compressed by about 94 and 97 %, in the particular systems under consideration that is, without any significant loss in resolution. More specifically, this implies that the numerical calculations are effectively reduced by about 94 and 97 %, respectively.

2 Theoretical Framework

2.1 Representation of Two-Body Interactions

We begin with treating the problem of finding a symmetry adapted representation of a two-body interaction in one dimension by first considering the two-body interaction of a set of particle densities on a line. The interaction is mediated by the two-body Gaussian potential

$$V_G^{(2)}(x_1, x_2) = \pm V_0^{(2)} \exp\left[-\left(\frac{x_1 - x_2}{a^{(2)}}\right)^2\right], \tag{1}$$

where the sign determines whether the force is attractive (-) or repulsive (+), $V_0^{(2)}$ sets the potential depth and $a^{(2)}$ is the range of the interaction. Even though the method is applicable to any central potential, this particular choice is motivated by the fact that, for instance, the Coulomb potential, can be expanded as a sum of Gaussian potentials [9]. Furthermore, we will consider a set of shifted particle densities of Gaussian type

$$\rho_n(x) = \rho_0 \exp\left[-\frac{1}{a}(x - x_n)^2\right], \tag{2}$$

where ρ_0 is the maxima of the density, x_n sets the center of the distribution and a determines the width. Each density can be interpreted as the density of a system of several particles, consequently, the integration of $\rho_n(x)$ will be equal to the total number of particles. For example, the densities could be the distribution of nucleons within a nucleus.

Each density will have a corresponding local Hartree potential $\Gamma_n^{(2)}(x)$ which is given by

$$\Gamma_n^{(2)}(x_1) = \int V_G^{(2)}(x_1, x_2)\rho_n(x_2)dx_2. \tag{3}$$

This is the potential experienced by a particle at x_1 due to all the other particles at x_2, described by the density $\rho_n(x_2)$. Lastly, the potential energy of a set of particles represented by the density $\rho_n(x)$ is [1]

$$E_n^{(2)} = \int V_G^{(2)}(x_1, x_2)\rho_n(x_1)\rho_n(x_2)dx_1dx_2. \tag{4}$$

2.1.1 Finding an Orthonormal Basis for the Space

The densities $\rho_n(x)$ together with their corresponding Hartree potentials $\Gamma_n^{(2)}(x)$ forms a space of states given by the, possibly non-orthogonal, set

$$\mathbf{\Phi} = \{\Phi_i(x)\} = \{\rho_1(x), \rho_2(x), \ldots, \rho_n(x), \Gamma_1^{(2)}(x), \Gamma_2^{(2)}(x), \ldots, \Gamma_n^{(2)}(x)\}. \tag{5}$$

We wish to orthonormalize this set using the canonical orthonormalization procedure [10], where the end result will be a set of orthonormal *natural states* $\mathbf{\Lambda} = \{\Lambda_k(x)\}$.

To begin with, let the sets $\mathbf{\Lambda}$ and $\mathbf{\Phi}$ be represented by column and row vectors respectively

[1] To be precise, the energy is given by $\frac{1}{2}$ of this due to double counting, but for the sake of simplicity, this will be ignored.

$$\begin{aligned}\boldsymbol{\Lambda}(x) &= [\Lambda_1(x)\ \Lambda_2(x)\ \ldots\ \Lambda_k(x)]^T \\ \boldsymbol{\Phi}(x) &= [\Phi_1(x)\ \Phi_2(x)\ \ldots\ \Phi_i(x)].\end{aligned} \tag{6}$$

The natural states are then given by

$$\boldsymbol{\Lambda}(x) = \boldsymbol{\Phi}(x)\mathbf{A}, \tag{7}$$

where $\mathbf{A}$ is a matrix such that

$$\begin{aligned}\int \boldsymbol{\Lambda}(x)^T\boldsymbol{\Lambda}(x)dx &= \int \left(\boldsymbol{\Phi}(x)\mathbf{A}\right)^T\left(\boldsymbol{\Phi}(x)\mathbf{A}\right)dx = \int \mathbf{A}^T\boldsymbol{\Phi}(x)^T\boldsymbol{\Phi}(x)\mathbf{A}dx \\ &= \mathbf{A}^T\left(\int \boldsymbol{\Phi}(x)^T\boldsymbol{\Phi}(x)dx\right)\mathbf{A} = \mathbf{A}^T\mathbf{O}\mathbf{A} = \mathbf{I},\end{aligned} \tag{8}$$

and the elements of the overlap matrix $\mathbf{O}$ are given by

$$O_{mn} = \int \Phi_m(x)\Phi_n(x)dx. \tag{9}$$

Eq. (8) has the general solution $\mathbf{A} = \mathbf{O}^{-1/2}\mathbf{U}$, where $\mathbf{U}$ is an orthogonal matrix that diagonalizes the overlap matrix $\mathbf{U}^T\mathbf{O}\mathbf{U} = \mathbf{D}$. Since $\mathbf{O}$ is symmetric and positive definite, all eigenvalues of $\mathbf{O}$ must be both real and non-negative [11]. We can therefore replace the elements of the diagonal matrix $\mathbf{D}$ by their square-root, giving us $\mathbf{D}^{1/2}$. This in turn lets us define the square-root of the overlap matrix as $\mathbf{O}^{1/2} = \mathbf{U}\mathbf{D}^{1/2}\mathbf{U}^T$, where $\mathbf{O}^{-1/2} = \left(\mathbf{O}^{1/2}\right)^{-1} = \mathbf{U}\mathbf{D}^{-1/2}\mathbf{U}^T$. We thus have that $\mathbf{A} = \mathbf{O}^{-1/2}\mathbf{U} = \mathbf{U}\mathbf{D}^{-1/2}$.

If the orthogonal matrix $\mathbf{U}$ consist of the normalized eigenvectors of $\mathbf{O}$, $\mathbf{D}^{-1/2}$ will have the inverse square root of the corresponding eigenvalues along its diagonal. Note that the eigenvalues of $\mathbf{O}$ are sorted in order of decreasing value $\lambda_1 \geq \lambda_2 \geq ... \geq \lambda_k$, and that the number of eigenvalues different from zero will be equal to the number of natural states N_{nat}. Finally, the solution to Eq. (7) is then

$$\boldsymbol{\Lambda}(x) = \boldsymbol{\Phi}(x)\mathbf{U}\mathbf{D}^{-1/2}, \tag{10}$$

or in component form

$$\Lambda_k(x) = \frac{1}{\sqrt{\lambda_k}}\sum_{i=1} U_{ik}\Phi_i(x), \tag{11}$$

where U_{ik} is the i'th component of the k'th eigenvector of $\mathbf{O}$ with eigenvalue λ_k and the sum runs over all the elements of $\boldsymbol{\Phi}$. Furthermore, the natural states span the smallest possible space that contains all the initial states in $\boldsymbol{\Phi}$. This space is refereed to as the *collective subspace* [12]. Moreover, while the set $\boldsymbol{\Phi}$ consists of localized particle densities and Hartree potentials, the set $\boldsymbol{\Lambda}$ instead consists of functions that are delocalized over the entire system, somewhat similar to Bloch wavefunctions describing a solid state system [10].

By studying the overlap between the natural states and the elements of $\mathbf{\Phi}$, one can infer the physical significance of the eigenvalues of $\mathbf{O}$. Let ω_k denote the overlap between the natural state $\Lambda_k(x)$ and all the elements of $\mathbf{\Phi}$, from Eq. (11) we then have that

$$\begin{aligned}\omega_k = \int \sum_j \Phi_j(x)\Lambda_k(x)dx &= \frac{1}{\sqrt{\lambda_k}} \sum_{j=1} \sum_{i=1} U_{ik} \int \Phi_j(x)\Phi_i(x)dx \\ &= \frac{1}{\sqrt{\lambda_k}} \sum_{j=1} \sum_{i=1} U_{ik} O_{ji}.\end{aligned} \tag{12}$$

The final sum on the right hand side is just the overlap matrix times its k'th eigenvector, which is just equal to eigenvector itself times the k'th eigenvalue. Squaring on both sides and using the fact that the eigenvectors are normalized we then have that $\omega_k^2 = \lambda_k$. Therefore, the eigenvalues are a measure of the overlap between the initial space $\mathbf{\Phi}$ and the natural states. Accordingly, the natural state corresponding to the largest eigenvalue will be the most important since it overlaps the most with $\mathbf{\Phi}$. Hence, why the eigenvalues are sorted in order of decreasing value.

For computational purposes it is also important to limit the number of eigenvalues considered to be non-zero since, from the numerical point of view, arbitrarily small eigenvalues will be regarded as non-zero. It is therefore common practice to impose a threshold ε such that only the eigenvalues satisfying $\lambda > \varepsilon$ are retained.

2.1.2 Expansion of the Two-Body Interaction In the Collective Subspace

The set of natural states $\mathbf{\Lambda}$, truncated to N_{nat} elements, is a linearly independent basis for the space. As such, the initial particle densities and corresponding Hartree potentials in $\mathbf{\Phi}$ can be expressed as a linear combination of the natural states,

$$\rho_n(x) = \sum_{i=1}^{N_{nat}} c_i^n \Lambda_i(x), \tag{13}$$

where

$$c_i^n = \int \Lambda_i(x_2)\rho_n(x_2)dx_2, \tag{14}$$

and

$$\Gamma_n^{(2)}(x) = \sum_{j=1}^{N_{nat}} d_j^n \Lambda_j(x). \tag{15}$$

We can use this fact in order to expand the two-body interaction in the collective subspace. Consider the form of the Hartree potentials as given in Eq. (3)

$$\Gamma_n^{(2)}(x_1) = \int V_G^{(2)}(x_1, x_2)\rho_n(x_2)dx_2. \tag{16}$$

We replace $\Gamma_n^{(2)}(x_1)$ by its expansion in the natural state basis

$$\sum_{j=1}^{N_{nat}} d_j^n \Lambda_j(x_1) = \int V_G^{(2)}(x_1, x_2)\rho_n(x_2)dx_2. \tag{17}$$

Using the orthogonality of the natural states we then multiply both sides by $\Lambda_k(x_1)$ and integrate over x_1 to solve for the coefficients d_j^n

$$\sum_{j=1}^{N_{nat}} d_j^n \int \Lambda_k(x_1)\Lambda_j(x_1)dx_1 = \int V_G^{(2)}(x_1, x_2)\Lambda_k(x_1)\rho_n(x_2)dx_1dx_2. \tag{18}$$

Since the integral on the left hand side is only non-zero for $j = k$ we have that

$$d_k^n = \int V_G^{(2)}(x_1, x_2)\Lambda_k(x_1)\rho_n(x_2)dx_1dx_2. \tag{19}$$

We then proceed by also expanding $\rho_n(x_2)$ in the collective subspace, resulting in

$$d_k^n = \sum_{k'=1}^{N_{nat}} c_{k'}^n \int V_G^{(2)}(x_1, x_2)\Lambda_k(x_1)\Lambda_{k'}(x_2)dx_1dx_2. \tag{20}$$

Introducing

$$\chi_{kk'} = \int V_G^{(2)}(x_1, x_2)\Lambda_k(x_1)\Lambda_{k'}(x_2)dx_1dx_2, \tag{21}$$

we can write this as

$$d_k^n = \sum_{k'=1}^{N_{nat}} c_{k'}^n \chi_{kk'}. \tag{22}$$

Observe that $\chi_{kk'} = \chi_{k'k}$, which is a direct consequence of the spatial exchange symmetry of the interaction. Furthermore, inserting the formula for the coefficient $c_{k'}^n$ into the equation above yields

$$d_k^n = \sum_{k'=1}^{N_{nat}} \chi_{kk'} \int \Lambda_{k'}\rho_n(x_2)dx_2. \tag{23}$$

Inserting this back into the expansion of $\Gamma_n^{(2)}(x_1)$ in the natural state basis we get

$$\Gamma_n^{(2)}(x_1) = \sum_{k=1}^{N_{nat}} \left[\sum_{k'=1}^{N_{nat}} \chi_{kk'} \int \Lambda_{k'}(x_2)\rho_n(x_2)dx_2 \right] \Lambda_k(x_1). \tag{24}$$

Since $\chi_{kk'}$ is just a number and $\Lambda_k(x_1)$ is independent of x_2, we can move them inside the integral

$$\Gamma_n^{(2)}(x_1) = \int \left[\sum_{k=1}^{N_{nat}} \sum_{k'=1}^{N_{nat}} \chi_{kk'}\Lambda_k(x_1)\Lambda_{k'}(x_2) \right] \rho_n(x_2)dx_2. \tag{25}$$

Comparing this with the definition of $\Gamma_n^{(2)}(x_1)$ as given by Eq. (16), we then have that the expression within the square brackets is equal to $V_G^{(2)}(x_1, x_2)$, that is

$$V_G^{(2)}(x_1, x_2) = \sum_{k=1}^{N_{nat}} \sum_{k'=1}^{N_{nat}} \chi_{kk'} \Lambda_k(x_1) \Lambda_{k'}(x_2). \tag{26}$$

This is then the expansion of $V_G(x_1, x_2)$ in the collective subspace. Moreover, consider performing singular value decomposition (SVD) on the $N_{nat} \times N_{nat}$ matrix $\mathbf{X}$ with elements $\chi_{kk'}$. This matrix is clearly symmetric since $\chi_{kk'} = \chi_{k'k}$ and the SVD therefore takes the following form

$$\mathbf{X} = \mathbf{U}\mathbf{\Sigma}\mathbf{V}^T = \left(\mathbf{U}\mathbf{\Sigma}\mathbf{V}^T\right)^T = \mathbf{V}\mathbf{\Sigma}\mathbf{U}^T \Longrightarrow \mathbf{X} = \mathbf{U}\mathbf{\Sigma}\mathbf{U}^T. \tag{27}$$

This can be written in terms of components as

$$\chi_{kk'} \approx \sum_{s=1}^{N} U_{ks} \sigma_s U_{k's} \quad \text{where} \quad N \leq N_{nat}. \tag{28}$$

If $N < N_{nat}$, $\chi_{kk'}$ is compressed, whereas if $N = N_{nat}$, $\chi_{kk'}$ is retrieved exactly. Consequently, the interaction is given by

$$\begin{aligned} V_G^{(2)}(x_1, x_2) &\approx \sum_{k=1}^{N_{nat}} \sum_{k'=1}^{N_{nat}} \sum_{s=1}^{N} U_{ks} \sigma_s U_{k's} \Lambda_k(x_1) \Lambda_{k'}(x_2) \\ &\approx \sum_{s=1}^{N} \left[\sum_{k=1}^{N_{nat}} \sqrt{\sigma_s} U_{ks} \Lambda_k(x_1) \right] \times \left[\sum_{k'=1}^{N_{nat}} \sqrt{\sigma_s} U_{k's} \Lambda_{k'}(x_2) \right]. \end{aligned} \tag{29}$$

We then define

$$Q^s(x) = \sum_{k=1}^{N_{nat}} \sqrt{\sigma_s} U_{ks} \Lambda_k(x), \tag{30}$$

allowing us to write

$$V_G^{(2)}(x_1, x_2) \approx \sum_{s=1}^{N} Q^s(x_1) \times Q^s(x_2), \tag{31}$$

which is a highly convenient representation of a two-body interaction. Note that the total number of singular values is equal to the number of natural states, and in the limit as N approaches N_{nat} the representation is exact in the collective subspace.

Furthermore, in order to quantitatively study the performance of this representation, we must first properly introduce what compression actually entails in our context. If we want to simulate the interaction of a set of particle densities on a one dimensional interval of length L, we would first have to partition this interval into a sequence of M equally distant points $\mathcal{P} = \{x_k\}_{k=0}^{M}$. To compute the two-body interaction we would then have to perform M^2

calculations, namely, Eq. (1) would have to be evaluated for all the points in $\mathcal{P}$. However, Eq. (31) only involves $M \cdot N$ computations, M times the number of unique $Q^s(x)$ functions that is, and the compression in units percent is therefore equal to $100(1 - N/M)$.

2.2 Representation of Three-Body Interactions

While the derivation of the representation of a generic three-body potential is similar to that of a two-body potential, there are some major differences. We begin with presenting the form of the three-body potential of interest, which is a finite-range Gaussian in one dimension

$$V_G^{(3)}(x_1, x_2, x_3) = \pm V_0^{(3)} \exp\left\{ \frac{1}{a^{(3)}} \left[-(x_1 - x_2)^2 - (x_1 - x_3)^2 - (x_2 - x_3)^2 \right] \right\}. \tag{32}$$

Though the shifted densities $\rho_n(x)$ remain unchanged, the corresponding Hartree potentials are instead given by

$$\Gamma_n^{(3)}(x_1) = \int V_G^{(3)}(x_1, x_2, x_3)\rho_n(x_2)\rho_n(x_3)dx_2dx_3. \tag{33}$$

They are similarly interpreted as the potential experienced by a particle at x_1 due to the average density of particles integrated over x_2 and x_3. The potential energy is [2]

$$E_n^{(3)} = \int V_G^{(3)}(x_1, x_2, x_3)\rho_n(x_1)\rho_n(x_2)\rho_n(x_3)dx_1dx_2dx_3. \tag{34}$$

Naturally, the deformed densities and Hartree potentials as given in Eq. (33) also forms a space, from which we then can obtain the collective subspace by the same procedure as above.

2.2.1 Expansion of the Three-Body Interaction In the Collective Subspace

Let $\mathbf{\Omega} = \{\Omega_i(x)\}$ denote the collective subspace in the three-body formalism. We can then likewise expand the initial states in terms of the natural states as expressed in Eq. (13) and Eq. (15). Doing so for the Hartree potential in Eq. (33) we then get

$$\sum_{i=1}^{N_{nat}} e_i^n \Omega_i(x_1) = \int V_G^{(3)}(x_1, x_2, x_3)\rho_n(x_2)\rho_n(x_3)dx_2dx_3. \tag{35}$$

Solving for the coefficient e_i^n as we did before results in

$$e_i^n = \int V_G^{(3)}(x_1, x_2, x_3)\Omega_i(x_1)\rho_n(x_2)\rho_n(x_3)dx_1dx_2dx_3. \tag{36}$$

We continue by also expanding $\rho_n(x_2)$ and $\rho_n(x_3)$ in the natural basis

[2] More specifically, a factor of $\frac{1}{6}$ would have to be included for this to be the actual energy, but this will be ignored in order to simplify matters.

$$e_i^n = \sum_{j=1}^{N_{nat}} \sum_{k=1}^{N_{nat}} f_j^n f_k^n \int V_G^{(3)}(x_1, x_2, x_3) \Omega_i(x_1) \Omega_j(x_2) \Omega_k(x_3) dx_1 dx_2 dx_3, \tag{37}$$

where we choose to denote the integral by χ_{ijk} and the coefficients f_j^n and f_k^n are as previously defined in Eq. (14). Hence,

$$e_i^n = \sum_{j=1}^{N_{nat}} \sum_{k=1}^{N_{nat}} \chi_{ijk} \left[\int \Omega_j(x_2) \rho_n(x_2) dx_2 \right] \times \left[\int \Omega_k(x_3) \rho_n(x_3) dx_3 \right]. \tag{38}$$

Plugging this into the expansion of $\Gamma_n^{(3)}(x_1)$ then results in

$$\Gamma_n^{(3)}(x_1) = \sum_{i=1}^{N_{nat}} \left[\sum_{j=1}^{N_{nat}} \sum_{k=1}^{N_{nat}} \chi_{ijk} \left[\int \Omega_j(x_2) \rho_n(x_2) dx_2 \right] \times \left[\int \Omega_k(x_3) \rho_n(x_3) dx_3 \right] \right] \Omega_i(x_1). \tag{39}$$

Rearranging, while taking into account that $\Omega_i(x_1)$ is independent of both x_2 and x_3 and that χ_{ijk} is just a number, yields

$$\Gamma_n^{(3)}(x_1) = \int \left[\sum_{i=1}^{N_{nat}} \sum_{j=1}^{N_{nat}} \sum_{k=1}^{N_{nat}} \chi_{ijk} \Omega_i(x_1) \Omega_j(x_2) \Omega_k(x_3) \right] \rho_n(x_2) \rho_n(x_3) dx_2 dx_3. \tag{40}$$

From which it is apparent that

$$V_G^{(3)}(x_1, x_2, x_3) = \sum_{i=1}^{N_{nat}} \sum_{j=1}^{N_{nat}} \sum_{k=1}^{N_{nat}} \chi_{ijk} \Omega_i(x_1) \Omega_j(x_2) \Omega_k(x_3). \tag{41}$$

Now, let χ_{ijk} be the elements of a third-order *cubical* tensor $\mathcal{X} \in \mathbb{R}^{N_{nat} \times N_{nat} \times N_{nat}}$, that is, it has three so-called *modes* of equal size. Modes being the same as dimensions, or equivalently, ways. This tensor is supersymmetric in the sense that it is invariant under permutations of its indices

$$\chi_{ijk} = \chi_{ikj} = \chi_{jik} = \chi_{jki} = \chi_{kij} = \chi_{kji} \quad \forall i, j, k \in \{1, ..., N_{nat}\}. \tag{42}$$

We would like to decompose this tensor using higher order singular value decomposition (HOSVD). This method is analogous to that of ordinary SVD but for tensors of arbitrary order. However, when the tensor is of order three, though not necessarily cubical, HOSVD is usually referred to as Tucker decomposition. Simply put, it entails decomposing the tensor into a *core tensor* which is multiplied by three matrices along each mode. This necessitates the introduction of two important concepts. First, the notion of *matrix unfoldings*, which is the process of reordering the elements of a tensor such that they form a matrix. Second, the *n-mode product*, which is the multiplication of a matrix along one of the modes of a tensor [13]. We begin with matrix unfoldings as it will be necessary to understand the n-mode product.

Let $\mathcal{A} \in \mathbb{R}^{I_1 \times I_2 \times ... \times I_N}$ be an arbitrary N-th order tensor, the n-mode matrix unfolding relocates the tensor element $a_{i_1 i_2 ... i_N}$ to the matrix element (i_n, j) of the matrix $\mathbf{A}_{(n)} \in \mathbb{R}^{I_n \times I_1 I_2 ... I_N}$, where

$$j = 1 + \sum_{k \neq n}^{N} (i_k - 1) \prod_{m \neq n}^{k-1} I_m. \tag{43}$$

Even though the definition is somewhat involved, the concept in itself is rather straightforward. For instance, consider a third-order tensor with dimensions $3 \times 2 \times 1$, it can then be unfolded into three different matrices with dimensions 3×2, 2×3 and 1×6, corresponding to the 1-mode, 2-mode and 3-mode unfolding respectively (see Appendix A). Moreover, and most importantly, if the tensor is cubical and supersymmetric, the unfoldings will all be equal [14]. This fact will be of great significance for us, as will be seen later.

We are now able to understand the n-mode product. Let $\mathcal{A}$ be the same tensor as above, the n-mode product of this tensor and a matrix $\mathbf{U} \in \mathbb{R}^{K \times I_n}$ is a new tensor $\mathcal{M} \in \mathbb{R}^{I_1 \times \ldots \times I_{n-1} \times K \times I_{n+1} \times \ldots \times I_N}$ and is denoted by

$$\mathcal{M} = \mathcal{A} \times_n \mathbf{U}, \tag{44}$$

or in component form

$$M_{i_1 \ldots i_{n-1} k i_{n+1} \ldots i_N} = \sum_{i_n=1}^{I_n} a_{i_1 \ldots i_N} u_{k i_n}. \tag{45}$$

This can also be expressed using matrix unfoldings

$$\mathbf{M}_{(n)} = \mathbf{U}\mathbf{A}_{(n)}, \tag{46}$$

that is, the matrix product of $\mathbf{U}$ and the n-mode unfolding of $\mathcal{A}$ is equal to the n-mode unfolding of the tensor $\mathcal{M}$, which is given by the n-mode product between $\mathbf{U}$ and $\mathcal{A}$. Additionally, it is also possible for a tensor to be multiplied by several matrices in a series of n-mode products. If the modes are different, it does not matter in which order the products are evaluated. To get better acquainted with these two concepts, please refer to Appendix A where explicit examples involving the n-mode product and matrix unfoldings are given.

Having introduced the n-mode product as well as matrix unfoldings, we are now in a suitable position to perform Tucker decomposition on $\mathcal{X}$. The Tucker form of $\mathcal{X}$ is given by

$$\mathcal{X} = \mathcal{G} \times_1 \mathbf{A} \times_2 \mathbf{B} \times_3 \mathbf{C}, \tag{47}$$

where $\mathcal{G}$ is the core tensor and $\mathbf{A}$, $\mathbf{B}$ and $\mathbf{C}$ are orthogonal matrices. These matrices can be obtained by performing ordinary SVD on the three matrix unfoldings of $\mathcal{X}$, where the acquired $\mathbf{U}$ matrices are orthogonal matrices. In fact, since $\mathcal{X}$ is supersymmetric, the three matrix unfoldings will be the same. Consequently, we have that $\mathbf{A} = \mathbf{B} = \mathbf{C} =: \mathbf{U}$ and the Tucker form of $\mathcal{X}$ is therefore given by

$$\mathcal{X} = \mathcal{G} \times_1 \mathbf{U} \times_2 \mathbf{U} \times_3 \mathbf{U}. \tag{48}$$

The core tensor can then be solved for as follows

$$\mathcal{G} = \mathcal{X} \times_1 \mathbf{U}^T \times_2 \mathbf{U}^T \times_3 \mathbf{U}^T. \tag{49}$$

Observe that $\mathcal{G}$ has the same dimensions and supersymmetry as $\mathcal{X}$. Moreover, the Tucker decomposition can be expressed in terms of components as

$$\chi_{ijk} \approx \sum_{I=1}^{N_I}\sum_{J=1}^{N_J}\sum_{K=1}^{N_K} G_{IJK}U_{iI}U_{jJ}U_{kK} \quad \text{where} \quad N_I, N_J, N_K \leq N_{nat} \tag{50}$$

and similarly for the core tensor

$$G_{IJK} = \sum_{i=1}^{N_{nat}}\sum_{j=1}^{N_{nat}}\sum_{k=1}^{N_{nat}} \chi_{ijk}U_{iI}U_{jJ}U_{kK}. \tag{51}$$

If the summation bounds N_I, N_J and N_K are equal to N_{nat}, the left and right hand side in Eq. (50) are exactly equal. Though, if $N_I, N_J, N_K < N_{nat}$ the tensor $\mathcal{X}$ is said to be compressed. At last, we now insert the Tucker form of χ_{ijk} into Eq. (41), which results in

$$\begin{aligned} V_G^{(3)}(x_1,x_2,x_3) &\approx \sum_{ijk}^{N_{nat}}\sum_{I=1}^{N_I}\sum_{J=1}^{N_J}\sum_{K=1}^{N_K} G_{IJK}U_{iI}U_{jJ}U_{kK}\Omega_i(x_1)\Omega_j(x_2)\Omega_k(x_3) \\ &\approx \sum_{I=1}^{N_I}\sum_{J=1}^{N_J}\sum_{K=1}^{N_K}\left[\sum_{i=1}^{N_{nat}} G_{IJK}^{1/3}U_{iI}\Omega_i(x_1)\right]\times\left[\sum_{j=1}^{N_{nat}} G_{IJK}^{1/3}U_{jJ}\Omega_j(x_2)\right] \\ &\times\left[\sum_{k=1}^{N_{nat}} G_{IJK}^{1/3}U_{kK}\Omega_k(x_3)\right]. \end{aligned} \tag{52}$$

We then define

$$Q^{IJK}(x) = \sum_{i=k}^{N_{nat}} G_{IJK}^{1/3}U_{kK}\Omega_k(x), \tag{53}$$

which is invariant under permutations of its first two indices due to the supersymmetry of the core tensor. This lets us write the interaction as

$$V_G^{(3)}(x_1,x_2,x_3) \approx \sum_{I=1}^{N_I}\sum_{J=1}^{N_J}\sum_{K=1}^{N_K} Q^{IJK}(x_1)\times Q^{JKI}(x_2)\times Q^{IKJ}(x_3). \tag{54}$$

Once again, it is interesting to study how many terms that needs to be included without any substantial loss of information. Also, when $N_I = N_J = N_K = N_{nat}$ the representation is exact in the collective subspace.

Moreover, due to the exchange symmetry of the two first indices in $Q^{IJK}(x)$, the number of unique $Q^{IJK}(x)$ functions that has to be calculated for $N_I = N_J = N_K = N$ will be equal to $N^2(N+1)/2$. Computing the interaction on a mesh line consisting of M points with the representation above would then require $M \cdot N^2(N+1)/2$ computations. In contrast, the standard form in Eq. (32) would instead require M^3 computations. The compression in unit percent is therefore be given by $100(1 - N^2(N+1)/2M^2)$.

3 Results

3.1 Convergence of the Representation of a Two-Body Interaction

3.1.1 Constructing The Collective Subspace

We begin with defining the space by using 60 shifted densities together with their corresponding Hartree potentials. The shifted densities are evenly spaced over an interval of length 10 fm and, consequently, so are the Hartree fields. This particular choice of space is motivated by its simplicity and was chosen such as to make the examination of the method as direct as possible. The space could be interpreted as the interaction of a set of one dimensional particle densities along a line. However, this rather unrealistic scenario carry no real physical significance and no useful predictions could be derived from it beyond what pertains to the performance of the method.

Furthermore, the interval was sub-divided into a mesh line consisting of 500 points. The space thus contains 120 elements, all of which are shown in Fig. (1). Note that some of the densities are abruptly discontinued at the ends of the interval, these are included in order to demonstrate that the method also works with discontinuous functions. The parameters used in the construction of the space are shown in Tab. (1).

Table 1: Parameters used to define the space.

ρ_0 [fm^{-3}]	a [fm^2]	$V_0^{(2)}$ [MeV]	$a^{(2)}$ [fm]
0.316	1.716	300.86	0.7

With these values for ρ_0 and a, the shifted densities correspond to the matter distribution in alpha particles with an rms radius of 1.61 fm [15]. The potential depth and range of the two-body interaction is adopted from [5].

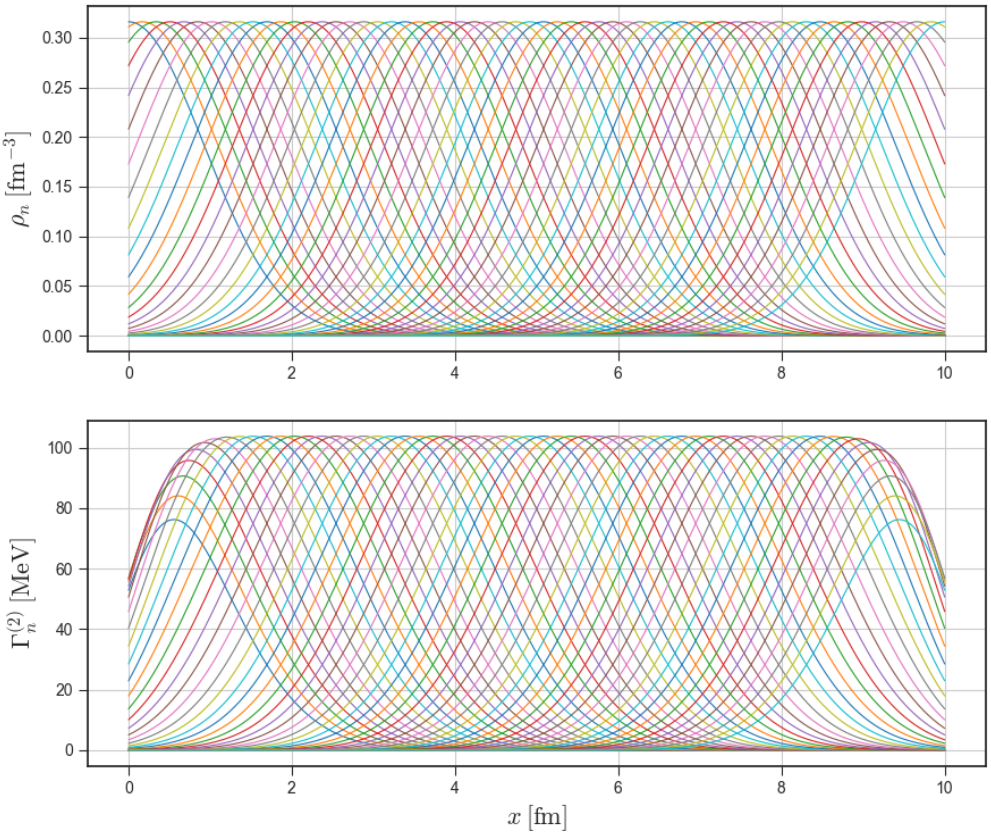

Figure 1: The space is defined by 60 shifted densities evenly spaced over a interval of length 10 fm together with their corresponding Hartree potentials. Top: the shifted densities $\rho_n(x)$. Bottom: Corresponding Hartree potentials $\Gamma_n^{(2)}(x)$.

By diagonalizing the 120×120 overlap matrix and retaining the eigenvalues above $\varepsilon = 10^{-13}$, the collective subspace was constructed. These eigenvalues were then sorted from largest to smallest before using Eq. (11) to build the collective subspace, which resulted in a total of 61 natural states. In Fig. (2) the natural states for $k = 1$, 2, 3 and 4 are plotted. We observe that these are indeed delocalized over the entire interval, as mentioned earlier, in contrast to the inital shifted densities and Hartree potentials, which are not. We also see some interesting trends in their shapes, for instance, the first state has one anti-node, the second has two and so on. In fact, their characteristics very much resembles those of simple standing waves. There is no actual explanation for this, though, it is not too surprising since any function can be expressed as a sum of sinusoidal functions in a Fourier sum.

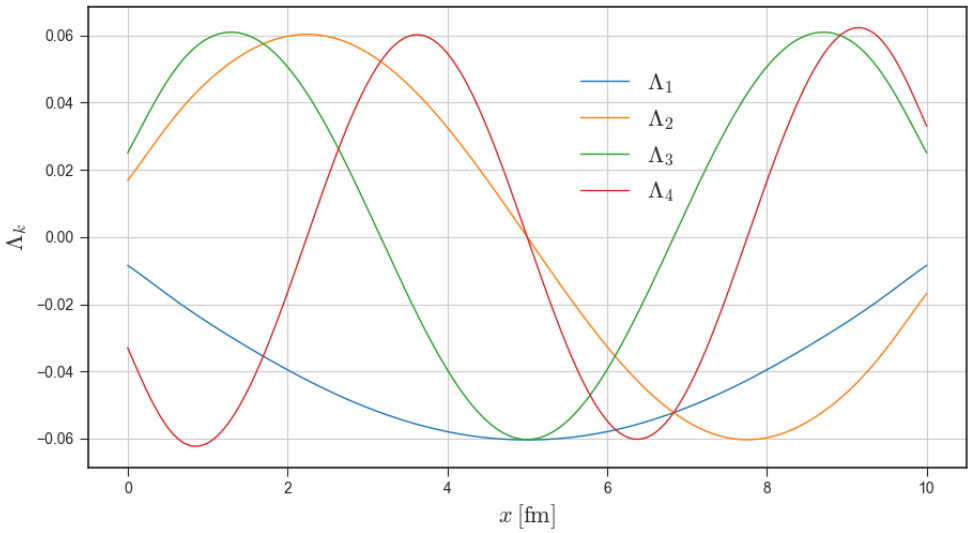

Figure 2: The first four natural states corresponding to the four largest eigenvalues.

3.1.2 Convergence of the Two-body Interaction In the Collective Subspace

Equipped with the collective subspace, we proceeded by solving for χ_{ij} using Eq. (21) and stored the values in a $N_{nat} \times N_{nat}$ (61×61) matrix $\mathbf{X}$. We then performed SVD on $\mathbf{X}$ and expressed it in component form using Eq. (28), which then allowed us to construct the $Q^s(x)$ functions needed to expand the interaction in the collective subspace in the form of Eq. (31). In Fig. (3), $Q^s(x)$ have been plotted for $s = 1, 2, 3$ and 4. It is apparent that there are a lot of similarities between the natural states shown in Fig. (2) and the set of $Q^s(x)$ functions shown in the figure below. This is a consequence of U_{ks} in Eq. (30) having very small values, except along the diagonal, such that $Q^s(x)$ filters out most of the natural states, beside the one corresponding to the index s.

Let us now analyze the performance of the decomposition as given by Eq. (31). In Fig. (4) the root-mean-square-logarithmic error (RMSLE), see Appendix B for definition, of the average energy is plotted for different values of N in Eq. (31). From this figure it is evident that the energy converges towards the exact value. The RMSLE also decreases linearly with N, first with one inclination and then with another more steeper. It then settles around $N = 27$, above which higher precision is unattainable. It is therefore unnecessary to consider terms above $N = 27$ since these do not reduce the error by any margin.

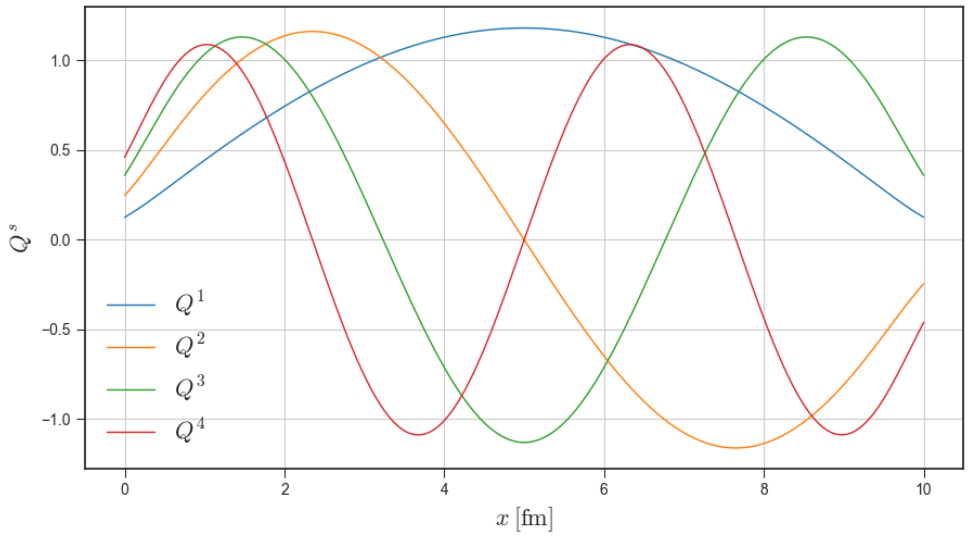

Figure 3: The first four $Q^s(x)$ functions corresponding to $s = 1, 2, 3$ and 4.

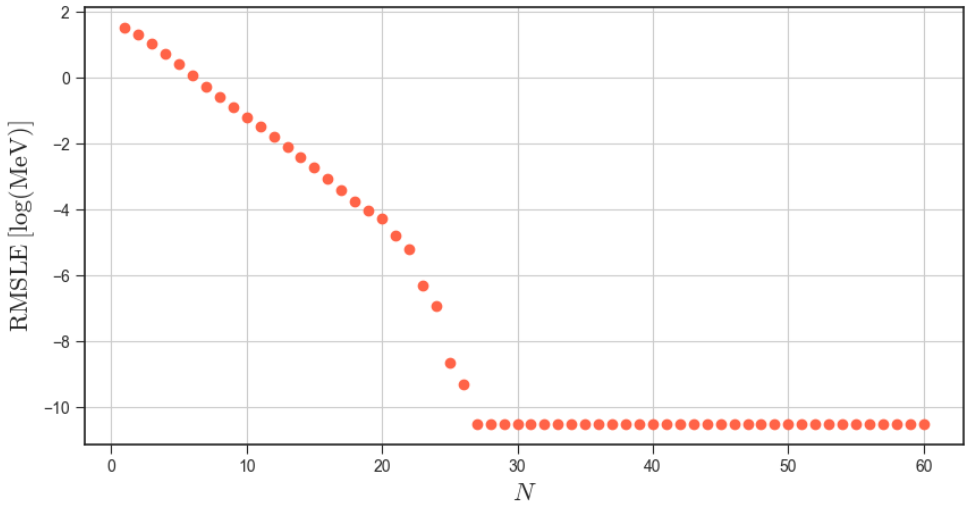

Figure 4: The root-mean-square-logarithmic error (RMSLE) of the average energy against the number of terms N in Eq. (31). In this figure all 61 natural states are used.

Moreover, in Fig. (5) the RMSLE of the average energy has been plotted against the amount of compression of the two-body interaction. From this figure, we see that a compression of around 95 % results in the interaction being fully retrieved, within the numerical precision of the algorithm, in the collective subspace. Generally, an error of around 10 keV is acceptable in practical calculations, which would correspond to a compression of about 97 %. Moreover, the time it takes to run many-body calculations is, for many methods, proportional to the information content of the interaction representation. Therefore, the obtained reduction in

information to about 3 % should correspond to the reduction in run time of full calculations applying the compression method.

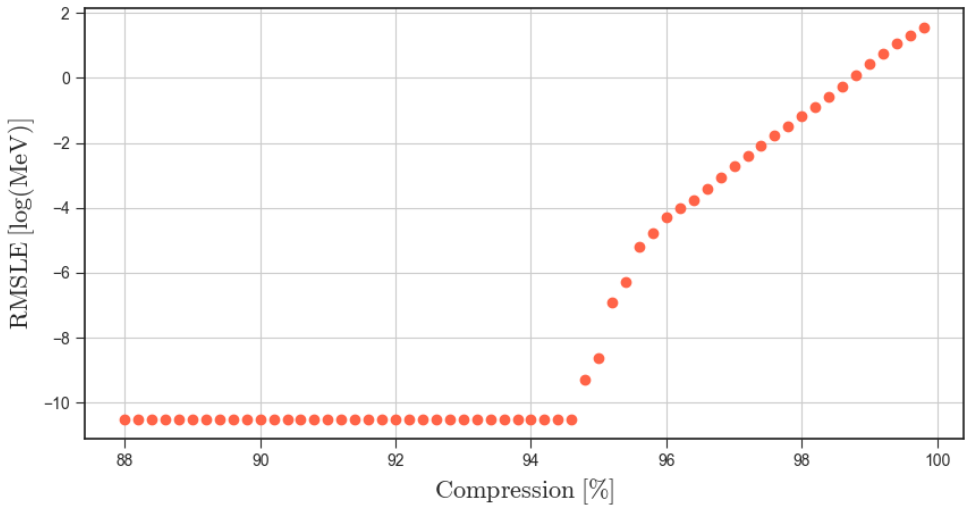

Figure 5: The root-mean-square-logarithmic error (RMSLE) of the average energy against the compression of the two-body interaction.

Lastly, in order to minimize the number of terms needed in Eq. (31) to attain the highest possible precision, it is fruitful to study the interplay between N and the number of natural states used, that is, N_{nat}. Hence, in Fig. (6) a heat map of the RMSLE of the average energy is shown with N on the vertical axis and N_{nat} on the horizontal axis. From this figure we observe some interesting features. Firstly, the upper triangular part is all yellow, signifying the fact that the maximum number of singular values is equal to the number of natural states. Secondly, for all values of N_{nat}, the minimum RMSLE is given by $N_{nat} = N$. In fact, increasing N_{nat}, while keeping N fixed, actually increases the RMSLE until it saturates, most notably so in the lower black region where the RMSLE is smallest. This is possibly due to the natural states deviating from their orthogonality as a result of numerical faults. To remedy this, it has been argued that choosing natural states based on their orthogonality, rather than discarding eigenvalues below a certain limit ε, is a more numerically stable method for constructing the collective subspace [16]. Lastly, we see that $N_{nat} = N = 25$ minimizes the number of terms needed in order to achieve the highest possible precision. Note, however, from Fig. (4) we previously got $N = 27$. This discrepancy is most definitely due to the collective subspace being inadequate, consisting of 61 natural states. Indeed, looking at Fig. (6), we see that for $N_{nat} > 38$ we can not enter the region where the RMSLE reaches its smallest value.

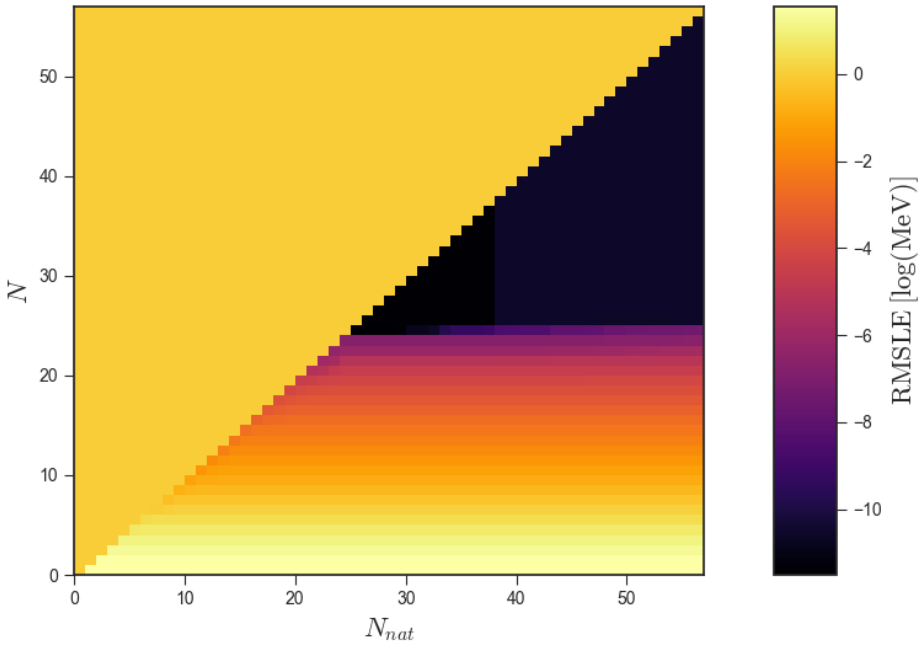

Figure 6: The root-mean-square-logarithmic error (RMSLE) of the average energy for different values of N and N_{nat}.

3.2 Convergence of the Representation of a Three-Body Interaction

3.2.1 Constructing The Collective Subspace

The space was built from 35 shifted densities, together with their corresponding Hartree potentials, and is shown in Fig. (7). The densities and Hartree potentials were defined over an interval of length 5 fm, which was sub divided into a mesh line consisting of 250 points. This somewhat smaller space was used such as to make computations less demanding. Furthermore, this space was chosen for the same reasons as in the two-body case, its simplicity. It also analogous to the space used in the two-body case, justifying the comparison between the performance of the representation of a two and three-body interaction respectively. The same values for ρ_0 and a as shown in Tab. (1) were used to construct the densities. The potential depth and range of the three-body interaction is shown Tab. (2) and was likewise adopted from [5].

The collective subspace, $\mathbf{\Omega}$, was similarly constructed by first diagonalizing the 70×70 overlap matrix, keeping only the eigenvalues greater than $\varepsilon = 10^{-10}$, and then applying Eq. (11). This resulted in a total of 38 natural states, the first four of which are plotted in Fig. (8). Their shapes can be seen to imitate those in Fig. (2), although, their amplitudes are slightly larger and their characteristics somewhat deviates from ordinary standing waves.

Table 2: Parameters used to define the three-body interaction.

$V_0^{(3)}$ [MeV]	$a^{(3)}$ [fm^2]
600	1.25

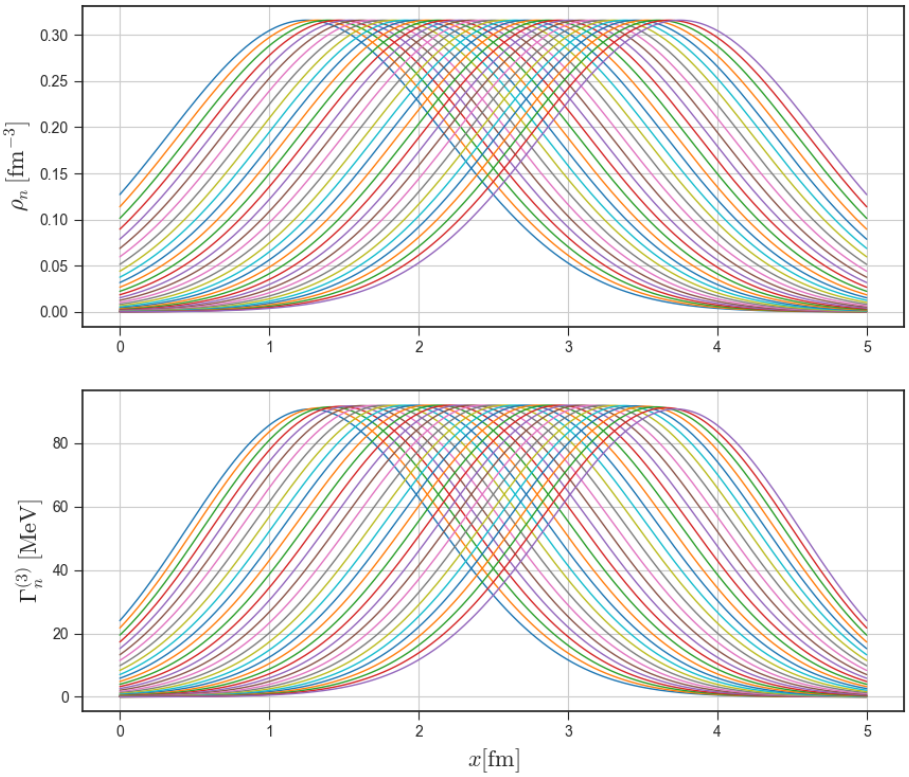

Figure 7: The space is defined, on a interval of length 5 fm, by 35 shifted densities and their corresponding Hartree potentials. Top: the shifted densities $\rho_n(x)$. Bottom: the Hartree potentials $\Gamma_n^{(3)}(x)$.

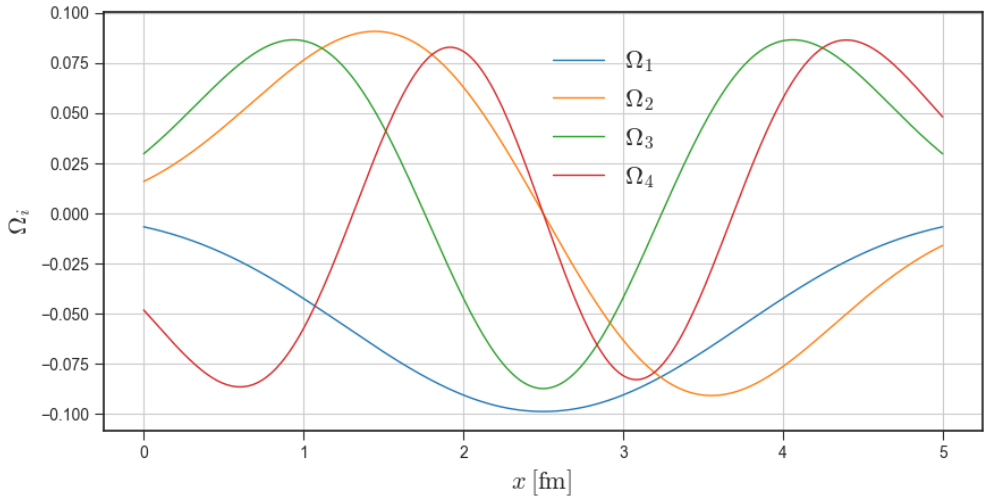

Figure 8: The first four natural states corresponding to the four largest eigenvalues of the overlap matrix.

3.2.2 Convergence of the Three-body Interaction In the Collective Subspace

We then continued by solving for the coefficients χ_{ijk} and stored the result in a $38 \times 38 \times 38$ tensor $\mathcal{X}$. The 1-mode matrix unfolding of this tensor was then calculated, resulting in a 38×1444 matrix $\mathbf{X}_{(1)}$. The orthogonal matrix $\mathbf{U}$ was then formed from the eigenvectors of the 38×38 matrix $\mathbf{X}_{(1)}\mathbf{X}_{(1)}^T$. The core tensor was thereafter calculated using Eq. (51), which ultimatedly allowed us to express χ_{ijk} in its Tucker form, namely, as in Eq. (50). Lastly, the $Q^{IJK}(x)$ functions was computed using Eq. (53) and the three-body interaction was represented as Eq. (54). In Fig. (9) a subset of $Q^{IJK}(x)$ functions are shown for different values of I with $J = K = 0$.

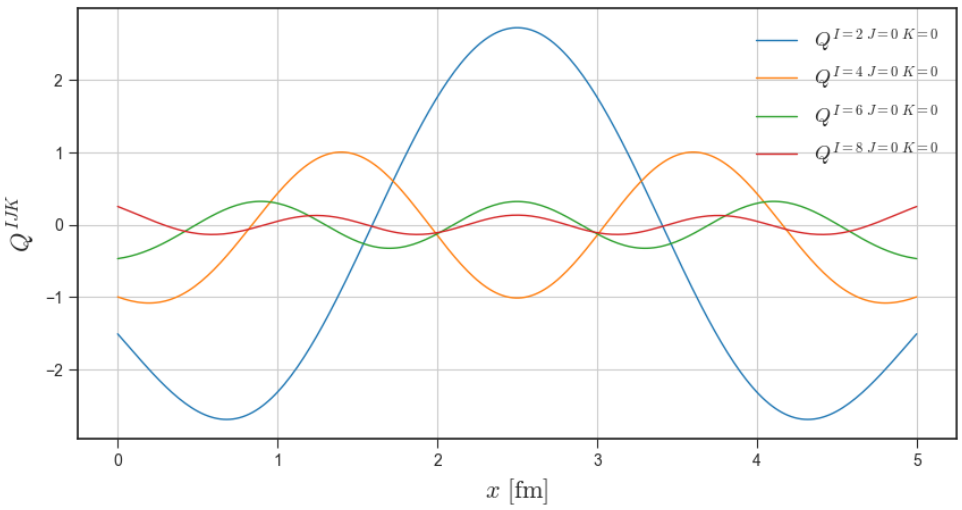

Figure 9: The $Q^{IJK}(x)$ functions for different values of I with $J = K = 0$.

In Fig. (10), the logarithmic absolute error (LAE) of the potential energy of the density centered at $x_n = 5/4$ has been plotted for different values of $N_I = N_J = N_K$. The behavior of this error is not as evident as for the two-body interaction. The error decreases somewhat linearly until it reaches a plateau, where it momentarily stops decreasing, and after this plateau is surpassed, the error starts decreasing again. In Fig. (10) two such plateaus can be seen, after which the error saturates at $N_I = N_J = N_K = 15$. Note that the number of terms in Eq. (54) is equal to $N_I \cdot N_J \cdot N_K$, and so, for the interaction to be exact in the collective subspace it appears that a total of 3375 terms would have to be included. In reality, since $Q^{IJK}(x)$ is symmetric under permutations of its first two indices, some of these terms would be equal and therefore unnecessary to compute more than once. Instead, one would only have to compute 1800 terms, which are unique, to reach the smallest error.

The ability of the representation in Eq. (54) to reduce the amount of numerical calculations is better appreciated by Fig. (11), where the LAE of the same density as in Fig. (10) is plotted against the compression of the interaction. We then see that a compression slightly above 97 % corresponds to the interaction being exact in the collective subspace, and with an error of around 10 keV, the interaction is compressed by almost 99.9 %.

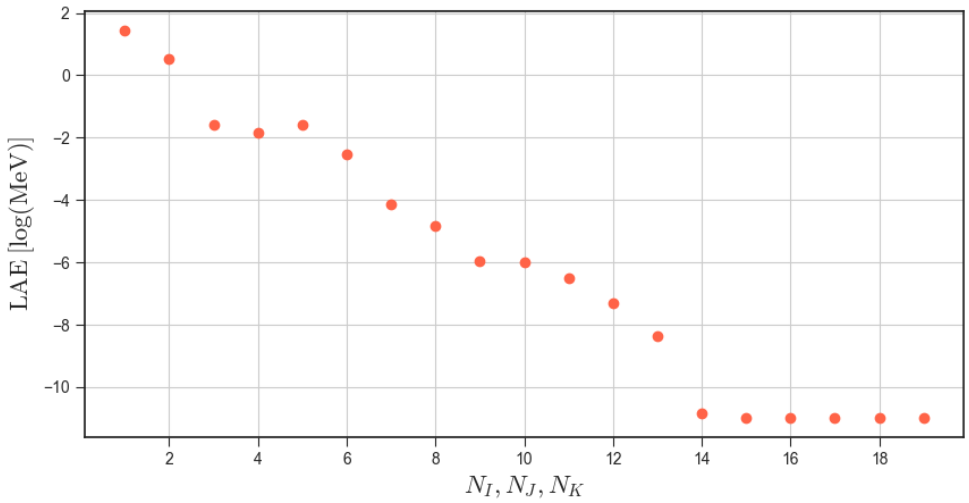

Figure 10: The logarithmic absolute error (LAE) of the potential energy of the density with $x_n = 5/4$ for different values of $N_I = N_J = N_K$. Observe that the number of terms in Eq. (54) is equal to $N_I \cdot N_J \cdot N_K$.

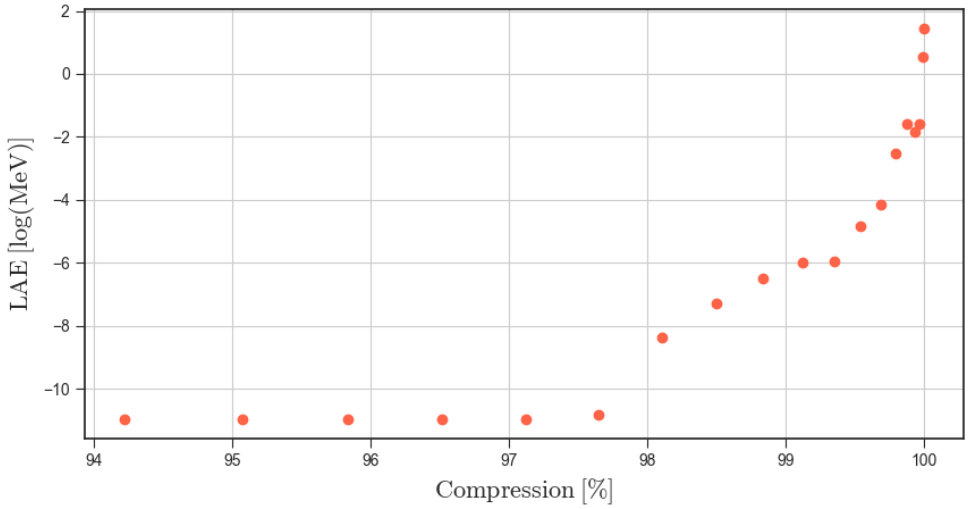

Figure 11: The logarithmic absolute error (LAE) of the potential energy of the density centered at $x_n = 5/4$ against the compression of the interaction for $N_I = N_J = N_K$.

4 Outlook

In conclusion, the performance of the symmetry adapted representation of a two-body interaction was analyzed in a system of one dimensional Gaussian particle densities. The results shows that the interaction under consideration could be compressed by about 94 % while still remaining exact in the collective subspace. It was also found that in order to optimize the resolution of the interaction, the number of singular values should be equal to the number natural states spanning the collective subspace. It is, however, unclear whether this applies more generally or if it is just the case in this particular instance.

Moreover, the corresponding representation of a three-body interaction was derived using Tucker decomposition and was similarly shown to be very proficient in compressing the interaction. A compression by about 97 % then resulted in the interaction being fully recovered in the collective subspace.

To put things in perspective, by a rough estimate, assume that the time it takes to run a realistic computation involving two and three-body interactions is proportional to the number of unique $Q(x)^s$ and $Q(x)^{IJK}$ in Eq. (31) and Eq. (54) respectively. For Eq. (31), the number of unique $Q(x)^s$ is simply equal to the upper bound in the sum. In Eq. (54), however, there will be $N^2(N+1)/2$ unique $Q(x)^{IJK}$ for $N_I = N_J = N_K = N$. We are then able to appreciate how much longer computations involving three-body interactions would take compared to two-body interactions if the same resolution is desired. For instance, in Fig. (4) we have that $N = 9$ is necessary in order to achieve an error of around 100 keV for two-body interactions. Likewise, by Fig. (10), an error slightly below 100 keV is attained for $N_I = N_J = N_K = 3$ in the three-body case. This translates into 18 unique $Q(x)^{IJK}$, and so, comparatively, the three-body calculation would roughly take twice as long. Similarly, an error of 10 keV requires 13 unique terms for the two-body case and 40 for the three-body case. Consequently, in this instance, the three-body calculation would take about 3 times

longer.

The method does, however, suffer from limitations in its current state. The symmetry adapted representation of a three-body interaction is not yet fully developed in three dimensions, neither is spin or isospin taken into account. Nevertheless, the results looks very promising and extending the method beyond these limitations is therfore highly warranted. Furthermore, the method could most likely be developed even further as to include higher-body interactions. After all, higher-body forces can equivalently be expanded in a collective subspace and tensors of arbitrary order can likewise be decomposed using HOSVD.

Acknowledgments

A lot of gratitude goes to Gillis Carlsson who proposed the subject of this thesis in the first place. I am extremely grateful for our discussions and your help throughout the entire work. Special thanks also goes to Andrea Idini whose assistance in revising this manuscript was truly invaluable.

Appendix A

Let $\mathcal{X}$ be a $(I_1 = 2) \times (I_2 = 2) \times (I_3 = 2)$ tensor with the 3-mode slices

$$\mathbf{X}_{i_1 i_2 1} = \begin{bmatrix} 1 & 2 \\ 3 & 4 \end{bmatrix} \tag{55}$$

and

$$\mathbf{X}_{i_1 i_2 2} = \begin{bmatrix} 5 & 6 \\ 7 & 8 \end{bmatrix}. \tag{56}$$

We wish to calculate the 1-mode unfolding of this tensor, which will result in a $I_1 \times (I_2 I_3) = 2 \times 4$ matrix $\mathbf{X}_{(1)}$. The tensor element $x_{111} = 1$ will map to the matrix element $(1, j)$, where by Eq. (43)

$$j = 1 + \sum_{k \neq 1}^{3} (i_k - 1) \prod_{m \neq 1}^{k-1} I_m = 1 + (i_2 - 1) \cdot 1 + (i_3 - 1) \cdot 2 = 1. \tag{57}$$

The tensor element $x_{221} = 4$ will map to the matrix element $(2, j)$, where

$$j = 1 + \sum_{k \neq 1}^{3} (i_k - 1) \prod_{m \neq 1}^{k-1} I_m = 1 + (i_2 - 1) \cdot 1 + (i_3 - 1) \cdot 2 = 2. \tag{58}$$

Performing the same operation on the 6 other tensor elements will then result in the matrix

$$\mathbf{X}_{(1)} = \begin{bmatrix} 1 & 2 & 5 & 6 \\ 3 & 4 & 7 & 8 \end{bmatrix}. \tag{59}$$

Furthermore, consider the 1-mode product of this tensor with the 2×2 matrix

$$\mathbf{U} = \begin{bmatrix} 2 & 2 \\ 2 & 2 \end{bmatrix}. \tag{60}$$

This will result in a new tensor $\mathcal{M}$, also of size $2 \times 2 \times 2$, and by Eq. (45) its elements are given by

$$M_{1 i_2 i_3} = \sum_{i_1 = 1}^{2} x_{i_1 i_2 i_3} u_{1 i_n} = x_{1 i_2 i_3} u_{11} + x_{2 i_2 i_3} u_{12} = 2 x_{1 i_2 i_3} + 2 x_{2 i_2 i_3} \tag{61}$$

and

$$M_{2 i_2 i_3} = \sum_{i_1 = 1}^{2} x_{i_1 i_2 i_3} u_{2 i_n} = x_{1 i_2 i_3} u_{21} + x_{2 i_2 i_3} u_{22} = 2 x_{1 i_2 i_3} + 2 x_{2 i_2 i_3}. \tag{62}$$

Hence, its 1-mode slices, which in this case incidentally are the same, are thus equal to

$$\mathbf{M}_{1 i_2 i_3}, \mathbf{M}_{2 i_2 i_3} = \begin{bmatrix} 8 & 24 \\ 16 & 30 \end{bmatrix}. \tag{63}$$

Appendix B

The RMSLE of the average potential energy is defined as

$$\text{RMSLE} = \log \sqrt{\frac{\sum_{i=1}^{N} (\hat{E}_i - E_i)^2}{N}}, \tag{64}$$

where N is the number of densities, $\hat{E}_i$ is the actual potential energy and E_i is the potential energy calculated using the representation. The LAE of the potential energy of a single density centered at x_n is given by

$$\text{LAE} = \log |\hat{E}_n - E_n|. \tag{65}$$

References

[1] S. C. Pieper and R. B. Wiringa. Quantum monte carlo calculations of light nuclei. *Annual Review of Nuclear and Particle Science*, 51(1):53–90, 2001.

[2] S. Drell and K. Huang. Many-body forces and nuclear saturation. *Physical Review*, 91:1527–1542, 1953.

[3] J. Fujita and H. Miyazawa. Pion Theory of Three-Body Forces. *Progress of Theoretical Physics*, 17(3):360–365, 03 1957.

[4] T.H.R. Skyrme. The effective nuclear potential. *Nuclear Physics*, 9(4):615–634, 1958.

[5] Y. Kanada-En'yo and Y. Akaishi. New effective nuclear forces with a finite-range three-body term and their application to antisymmetrized molecular dynamics. *Phys. Rev. C*, 69:034306, Mar 2004.

[6] H. Hammer, A. Nogga, and A. Schwenk. Colloquium: Three-body forces: From cold atoms to nuclei. *Rev. Mod. Phys.*, 85:197–217, Jan 2013.

[7] V. Efimov. Energy levels arising from resonant two-body forces in a three-body system. *Physics Letters B*, 33(8):563–564, 1970.

[8] B.G Carlsson et al. to be submitted.

[9] B.G Carlsson. communications.

[10] P. Löwdin. On the nonorthogonality problem*. volume 5 of *Advances in Quantum Chemistry*, pages 185–199. Academic Press, 1970.

[11] J. Liguang and H. Yew. Application of löwdin's canonical orthogonalization method to the slater-type orbital configuration-interaction basis set. *International Journal of Quantum Chemistry*, 115, 04 2015.

[12] P. Ring and P. Schuck. The Nuclear Many-Body Problem, pages 400–404. *Springer-Verlag Heidelberg*, study edition, 1980.

[13] T. G. Kolda and B. W. Bader. Tensor decompositions and applications. *SIAM Review*, 51(3):455–500, 2009.

[14] L. D. Lathauwer, B. D Moor, and J. Vandewalle. A multilinear singular value decomposition. *SIAM J. Matrix Anal. Appl.*, 21(4):1253–1278, mar 2000.

[15] Y. Eisen, B. Day, and E. Friedman. Microscopic description of the real alpha-nucleus potenial at large distances. *Physics Letters B*, 56(4):313–317, 1975.

[16] J. Martínez-Larraz and T. R. Rodríguez. Optimization of the number of intrinsic states included in the discrete generator coordinate method. *Physical Review C*, 106:054301, Nov 2022.